Two fuel performance codes of the PLEIADES platform: ALCYONE and GERMINAL

Bruno Michel, Isabelle Ramière, Isabelle Viallard, Clément Introini, Marc Lainet, Nathalie Chauvin, Vincent Marelle, Antoine Boulore, Thomas Helfer, Renaud Masson, et al.

Two fuel performance codes of the PLEIADES platform: ALCYONE and GERMINAL

B. Michel, I. Ramière, I. Viallard, C. Introini, M. Lainet, N. Chauvin, V. Marelle, A. Boulore, T. Helfer, R. Masson, J. Sercombe, J.C. Dumas, L. Noirot and S. Bernaud

CEA, DES, IRESNE, DEC, Cadarache F-13108, Saint-Paul-Lez-Durance, France

9.1 General overview of the PLEIADES fuel software environment

9.1.1 Architecture and generic tools for fuel performance codes

The PLEIADES software environment is a simulation framework allowing the development of fuel performance codes dedicated to specific nuclear systems [Pressurized Water Reactor (PWR), Sodium Fast Reactor (SFR), and Material Testing Reactor (MTR)], experimental devices, and advanced fuel modeling.

This platform is based on the C++ language. The kernel of the platform, called the architecture, provides generic tools for multiphysics algorithms, data exchange (SALOME [1]), multidimensional thermomechanical solver (Cast3m finite element code [2]), and the link with fuel databases. User-friendly interfaces are available for pre- and postprocessing within SALOME. The development method in the PLEIADES platform is based on a continuous integration process based on Jenkins. Thanks to this process, an automatic nonregression test database can be run after each commit in the version control system.

The PLEIADES software environment provides also the open-source MFront tool [3] for the implementation and storage of all the material properties and behavior laws. This tool includes a common numerical library to solve nonlinear differential constitutive equation systems associated with the mechanical behavior.

ALCYONE and GERMINAL are the fuel performance codes of the PLEIADES platform, devoted, respectively, to PWR and SFR fuel rod type concepts. For these two codes, a

qualification status, based on verification, validation, and uncertainties, is provided to the users for their studies. ALCYONE and GERMINAL codes validation is based on various experimental programs including irradiations in French power nuclear reactors (see Refs. [4–7]). Simulation results and modeling are also discussed in the framework of several international programs [8–11].

9.1.2 Multiphysics computational scheme for fuel rod type geometries

9.1.2.1 Algorithm

For fuel rod type geometries, a generic multiphysic computational scheme is proposed in the PLEIADES platform. Main features of this computational scheme are illustrated in Fig. 9.1. A time incremental formulation where a set of fixed point coupling resolutions at different scales or stages are achieved to compute the multiphysic fuel rod behavior for each time step. These fixed point algorithms are block Gauss–Seidel algorithms where each model is called sequentially within a convergence loop. Acceleration algorithms [12] are commonly used to fasten the slow linear convergence of the standard fixed point iterations. The time marching can be a priori given or automatically adjusted during the calculation. Two main scales are considered, respectively, named "global" and "local." At the local scale a recursive coupling algorithm is also possible to compute physical state variables involving a multi scale approach (see for instance Section 9.2.2.6 with the microscopic and macroscopic square finite element approach implemented in ALCYONE).

9.1.2.2 Global scale

This scale describes the behavior of the whole fuel rod with a fixed point algorithm between the axial discretization in slices and the 0D models for the uniform state variables

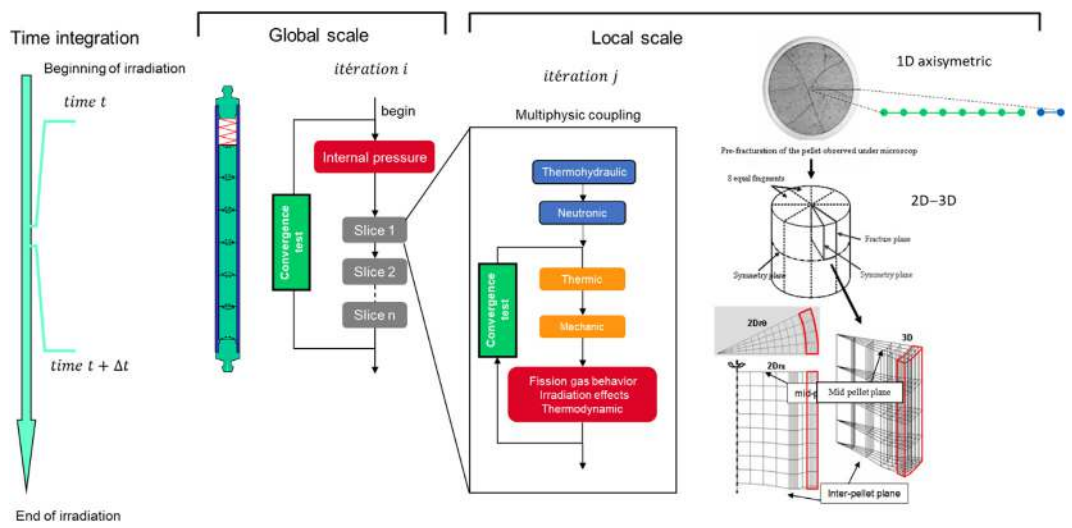

FIGURE 9.1 PLEIADES generic computational scheme for fuel rod type geometries.

in the fuel rod. These state variables can be, for instance, fuel rod internal pressure or total fission gas release (FGR).

9.1.2.3 Local scale

The local scale describes the multiphysic behavior of one slice composed of a stack of pellets and associated piece of cladding. The slice behavior is derived from an axial homogenization assumption where a single pellet located in the middle of the axial slice is represented. Different geometrical assumptions can be used to describe the local behavior from one-dimensional (1D) axisymmetric up to a two-dimensional (2D) or three-dimensional (3D) representation of one or several pellet fragments (see Fig. 9.1). The local state variables are stored and computed with fields associated to a mesh representing the pellet, the gap, and the cladding. In the multiphysics coupling scheme at local scale two types of models can be called: spatial models (e.g., thermic and mechanic) or point models (fission gas behavior, simplified neutronic model, swelling, etc.). The spatial thermal and mechanical equilibria are solved with the Cast3M finite element code. Point models are usually based on nonlinear ordinary differential equation (ODE) systems. These constitutive equations are derived from a multiscale description of the physicochemistry of irradiation. Among these point models, a Calphad Solver [13] is also available, in the PLEIADES environment, in order to assess the thermodynamic equilibrium under irradiation.

9.1.2.4 Software implementation

The fuel rod computational scheme is implemented thanks to the coupling tools provided by the PLEIADES architecture. These tools are generic functions describing fixed point algorithms illustrated in Fig. 9.1. Among these generic tools, we can have for instance:

- global coupling, global Model: to describe physical coupling at the fuel rod scale
- local coupling, local model: to describe the physical coupling at the slice scale
- objects linked to the fixed point convergence assessment: convergence criterion, acceleration algorithm, and prediction algorithm
- time step evaluation functions (available as a model methods) for the automatic management of the time marching: time step prediction and time step subdivision (in case of nonconvergence).

9.1.3 Verification process and quality control for the fuel performance codes of the PLEIADES platform

The verification process is based on the software quality control and on the unit and integral nonregression tests. Verification is performed after each commit in the version control system thanks to the Jenkins tool. Nonregression verifications are achieved through a comparison between two text files (the reference and the new one) structured under a multicolumn format. Relative, absolute, or mixed error criteria can be selected for each pair of columns. All the process, test execution and comparison, is automatized with a script file located in each folder containing the input files and the reference results of a verification test.

9.1.3.1 *Software quality control*

In the PLEIADES software environment, programing rules are recommended for the different languages available in the platform. An automatic verification of the use of these programming rules in the source code can be done with the tools Cpplint and Clang-Tidy. In order to check the fraction of the source code covered by the nonregression tests, open-source codes GCOV and LCOV are available in the platform. This verification can also be done with an automatic process through the Jenkins tools and a code coverage report is available at the end.

9.1.3.2 *Unit nonregression tests*

These tests are possible thanks to a unit computational scheme called "SKEL" provided by the PLEIADES software environment. With "SKEL" each physical model can be executed separately with all the input data defined in an "xml" file. So, a unit test can be done for a single time step with a "global scale" model or a "local scale" model (see Sections 9.1.2.2 and 9.1.2.3). For the "local scale," it can be either a point model or a spatial model. For a complete verification of nonlinear models the source code coverage tool can help to select enough time steps. In the case of unit verification tests the reference results can be derived from an analytical solution or from a reference computation with another code. Experimental results of unit tests are not used at the verification stage but are used for the separate effect validation with the fit of some material parameters.

9.1.3.3 *Integral nonregression tests*

These tests are achieved with a complete execution of the fuel performance code. These integral nonregression tests are composed of a representative sample of the validation data base. This representative sample has to be defined according all the computational schemes implemented in the fuel performance code (see source code coverage in Section 9.1.3.1) and in order to cover the entire validation domain. In the case of integral verification tests the reference results refer to a previous validated version of the fuel performance code. The reference results have to be updated when the computation-experiment comparison is improved.

9.2 ALCYONE fuel performance code for GEN II and III

9.2.1 General presentation

The ALCYONE [14] code is dedicated to the modeling of the in-reactor behavior of PWR fuel rods during normal (base irradiation) and off-normal (power ramps and accidental situations) operating conditions and incorporates several calculation schemes (Table 9.1). A 1D reference scheme, based on a 1D axi-symmetric description of the fuel element associated to a discrete axial decomposition of the fuel rod in stacked independent fuel slices, is used to study the behavior of the complete fuel rod. A 2D scheme that describes pellet-cladding interaction (PCI) at the mid-pellet (MP) plane of a pellet fragment is available to assess precisely stress concentration in the cladding near a pellet crack tip [15]. A 3D model of the complete pellet fragment and overlying cladding is also

TABLE 9.1 Computational schemes available in the ALCYONE fuel performance code.

Loading conditions	Modeling	Local model dimension	Neutronic	Thermohydraulic	Thermic	Mechanic	Fission gas behavior	He behavior	Thermodynamic
Nominal and power ramp	Standard	1D 2D (r, theta) 3D	Prodhel	1D homogenized two-phase flow	Cast3M		CARACAS	RACHEL	Open Caphad
RIA				1D two phase flow and post-DNB					
LOCA		1D		convection and radiation heat transfer					
Nominal and power ramp	Advanced	1D		1D homogenized two-phase flow			MARGARET		

1D, One-dimensional; *2D*, two-dimensional; *3D*, three-dimensional.

of interest when detailed studies of PCI are required [16]. Moreover, two advanced schemes (MARGARET and RACHEL) for UO_2 and MOX fuels can be used in 1D. MARGARET [17] is an advanced gas model, which describes more precisely gas diffusion and gas release in the fuel, and RACHEL is a model dedicated to helium release. Finally, transient schemes are used to simulate accidental situations with the activation of specific models and constitutive laws. One of the key features of ALCYONE is the integration of a thermochemical model, which is very useful to predict cladding failure during PCI power ramps.

9.2.2 Physical models

9.2.2.1 Isotopic vector evolution and nuclear reactions products

The isotopic vector evolution and nuclear reactions products, including fission, are computed with a 1D axisymmetric neutronic model [18]. This model consider an assumption of a one group of energy homogenization based on a conservation principle of the mean nuclear reaction rate in the pellet as a function of the pellet. The input of this model are the linear power and the one energy group mean cross section both given by a multigroup neutronic computation including the Boltzmann transport equation at assembly scale or core scale. Outputs of the PRODHEL model are the power density and the nuclear reactions products concentration as a function of the radius and time. This model includes all the data to compute Helium production in the reactor core or under storage.

9.2.2.2 Fission gas behavior and helium release

The fission gas models in ALCYONE represent all the physical and microstructural evolution of the fuel induced by fission gases under different irradiation conditions, including nominal, transient, and accidental loadings. They have been developed with a large experimental database which gather post irradiation examination and in situ measurement results for base irradiations up to high burn up, power ramp tests and annealing tests [19−22]. The model constitutive equations, based on a mean spherical grain assumption for the diffusion process, are defined with a set of state variables that represent the fission gas behavior according all the mechanisms identified through postirradiation examination [21], separate effect experiments [23], and simulation [24].

Microstructure evolution and fission gas localization assessment includes the fundamental features of fission gas behavior, among which are gas creation, diffusion, precipitation in fuel grains, gas resolution from bubbles, growth and coalescence of gas bubbles at grain faces, grain growth, as well as steady-state and transient gas release. For intra- and intergranular behaviors description the physical state variables are the bubble density, bubble size, gas concentration in bubbles, and dissolved in the fuel lattice. These state variables give an accurate description of the microstructure radial gradient induced by irradiation. More complex microstructure evolutions such as the precipitation zone are achieved through a bimodal bubble radius population in MARGARET [17]. The main difference between the two approaches is the nanometric bubbles precipitation. A physical mechanism of precipitation is represented in MARGARET whereas CARACAS approach is based on experimental quantified data. The High Burn Structure zone development is also

described with a continuous transition thanks to an heterogeneous approach including a partially restructured state [17,25]. A specific model of intergranular fragmentation due to over pressurized intergranular bubbles has been developed in both approaches for LOCA conditions.

The partial derivatives equations, associated to the intragranular diffusion, are solved with a finite volume method. A complete ODE system is then built with the discretized finite volume system and all the balance equations used to describe fission gas behavior. The number of state variables is adjusted depending on the irradiation condition in order to optimize the number of unknown. A continuous transition between different irradiation conditions (for instance steady state and accidental conditions) can be obtained through a dynamic evolution of the size of the ODE system and appropriate initialization process. FGR and fuel swelling assessments have been compared to experimental results for a large data base devoted to the integral validation of the ALCYONE fuel performance code.

RACHEL provides an integrated modeling of helium behavior during nominal and transient irradiations of the fuel. The model takes into account helium diffusion with trapping and resolution from intra- and intergranular cavities described by the fission gas model CARACAS. Contrary to fission gases, helium is slightly soluble in the fuel, then diffusion and infusion between intragranular dissolved He, intergranular dissolved He, and free volume are modeled too. Furthermore, a sizeable collection of helium-release measurements, at the end of irradiations, allows calibration and validation of RACHEL model.

9.2.2.3 Thermochemical analysis and corrosive fission products release

Chemistry of volatile fission products (FP), such as cesium Cs, iodine I, and tellurium Te, is of some importance with regards to PCI failures of the cladding by iodine stress corrosion cracking (I-SCC) [26] in transient conditions (class 2 power ramp). A realistic thermo-chemical-mechanical modeling of PCI/I-SCC is now possible thanks to the sophisticated models integrated in the PLEIADES/ALCYONE fuel performance code. In particular, the multiphysics coupling scheme of PLEIADES includes the neutronics model PRODHEL [18], the inert FGR model MARGARET [17], and the OpenCalphad (OC) thermochemical solver [13] which enables one to estimate the FPs inventory and to describe precisely their chemical association and their migration/release in gaseous form from the fuel during irradiation. The three main steps of this thermochemical calculation can be detailed as follows:

- The first step is to calculate at each node of the Finite Element mesh the FPs inventory with PRODHEL from a 1D radial neutron model using one-group burn up−dependent cross-sectional data. The neutronics model PRODHEL considers the chains of actinides (U, Pu, Am, Cm, and Np) and the FPs (Xe, Kr, Cs, Rb, I, Br, Te, Se, Mo, Tc, Ru, Rh, Pd, Sr, Ba, Y, La, Nd, Pm, Eu, Gd, Ce, Pr, Nb, and Zr). Overall, it includes 199 isotopes of FPs and 23 isotopes of actinides. Only isotopes having a significant impact on the isotopic inventory are considered, namely, those with neutronics cross sections above 0.1 barn. For the sake of simplification of the equilibrium calculations, actinides and FPs having similar behavior are grouped according to chemical families (e.g., inert fission gas, volatile FPs, stable oxides, metallic FPs, actinides, and FPs in solid solution in UO_2) with one representative element for each of them.

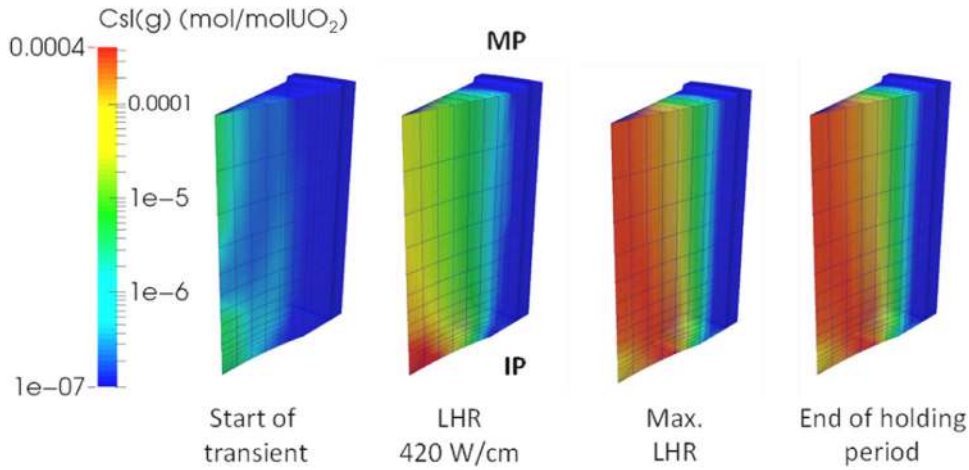

FIGURE 9.2 Assessment of the gaseous species amount for the CsI chemical compound during a power ramp transient in ALCYONE.

- The second step is to calculate at each node of the Finite Element mesh the local chemical equilibrium state of the FPs from the inventory provided by the model PRODHEL. For this purpose an extensive thermodynamics database containing all the phases and chemical species that are likely to form in the fuel in a gaseous, solid, or liquid states is required, such as the *Thermodynamics of Advanced Fuels – International Database* (TAF-ID) [27,28]. In PLEIADES the OC thermochemical solver is used to calculate the equilibrium state at constant pressure and temperature by minimizing the Gibbs energy under mass balance constraint and, for phases with ions, under an additional charge balance constraint [13]. The outputs are the concentrations of all the phases and species formed at equilibrium: fluorite phase, gaseous species, condensed species, metallic precipitates, and liquid phases) (see illustration in Fig. 9.2), the oxygen-to-metal ratio in the bulk but also in the fluorite phase, the chemical potentials of each element and thermodynamic properties such as the heat capacity.
- The third step is to take into account the transport of the FPs and their release from the fuel. A reasonable estimate of FPs release can be obtained in simulations of power ramp by considering that only the gas species formed in the fuel are released, showing, therefore, the importance of fuel thermochemistry. To avoid a complex coupling with the inert Fission Gas model MARGARET, an FP gas species release rate proportional to the inert FGR from grain faces has proved to give good results [29].
- In recent years, another phenomenon of importance for fuel thermodynamic equilibrium calculations has been integrated in the PLEIADES/ALCYONE [29,30]: oxygen thermodiffusion. In fact, oxygen radial redistribution in the fuel driven by the thermal gradient strongly modifies local thermochemical equilibria at the pellet center and leads to the release of a large amount of gaseous cesium which, in turn, can limit PCI failure propensity by reacting with iodine in the free volume of the fuel rod [31].

9.2.2.4 Crack extension modeling in fuel

9.2.2.4.1 Macroscopic scale

Crack extension at macroscopic scale is considered in the fuel in order to assess stress relaxation and pellet fragment relocation induced by the material rupture. In ALCYONE crack-extension assessment is included in the nonlinear finite element mechanical model through two different aspects: a direct description of the pellet fragment with a mesh and a smeared crack model [32,33] based on a continuum damage approach. The first aspect concerns only 2D and 3D models where primary cracks, occurring the first power increase, are explicitly meshed with appropriate boundary conditions. The smeared crack model is used in 1D, 2D, and 3D in order to describe crack initiation and growth depending on the stress and strain states evolution under irradiation.

9.2.2.4.2 Microscopic scale

Crack extension at microscopic scale is considered in the fuel in order to assess grain boundary separation involved in FGR or a pellet over fragmentation process under accidental loading. In ALCYONE microcracks extension are introduced in the fission gas model through a simplified equation depending on the macroscopic mechanical state and on the stable fission gases pressure. These simplified models are derived from experimental results and from 3D full field computation achieved with the "reference volume element" application of the PLEIADES platform.

9.2.2.5 Heterogeneous mechanical behavior

For heterogeneous Pu content microstructures, homogenized mechanical models are available in ALCYONE. Initially formulated to model the fuel behavior during normal operating conditions (see Refs. [34,35]), this work has been extended to model the fuel behavior during off-normal operating conditions [36]. For these models the computational scheme enables a two-scale coupling formulation between gaseous swelling and nonlinear mechanical behavior [37]. The homogenized mechanical model provides macroscopic and microscopic stress−strain states according heterogeneous gaseous swelling and heterogeneous creep properties of the material. The microscopic stress state can then be used through the coupling formulation to assess heterogeneous gaseous swelling.

9.2.2.6 Multidimensional and multiscale analysis

The multidimensional analysis proposed in the ALCYONE is based on a continuous formulation at the pellet fragment scale for the thermal and the mechanical behaviors coupled with the same multiphysic equations than the ones derived for the 1D fuel performance codes. The computational scheme available [14] is a single pellet approach where boundary conditions for the coolant temperature and fuel rod internal pressure are given by a preliminary 1D computation. An illustration of the elementary finite element mesh used for the 3D model is given in Fig. 9.3. In this approach, each pellet fragment is represented with a simplified "piece of cake" type geometry, and mechanical interaction between the pellet and the cladding and with other pellet fragments is taken into account with unilateral contact conditions. Thanks to this elementary 3D model, several pellet

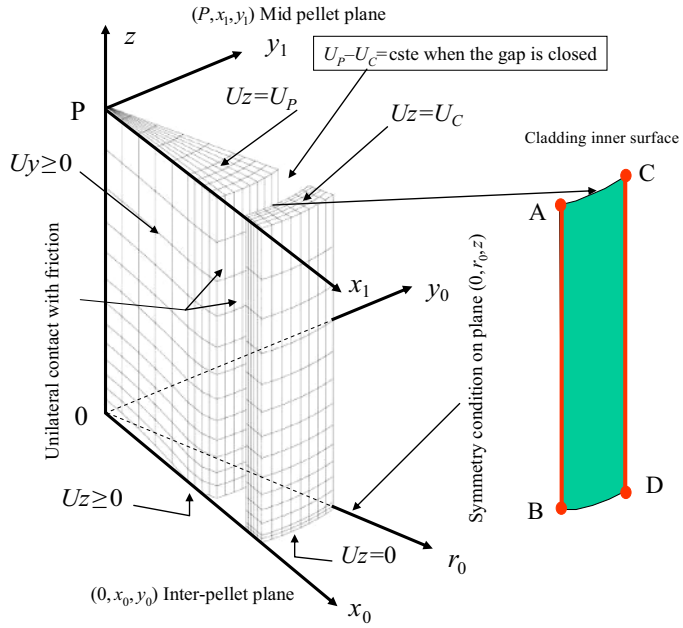

FIGURE 9.3 3D finite element mesh for PCI: symmetries and boundary conditions. *PCI*, Pellet-cladding interaction.

fragments can be represented in order to study a fraction of the pellet or a small stack of pellet fragments.

The thermomechanical problem is solved with the Cast3M finite element code for a general continuous formulation presented here after.

9.2.2.6.1 Thermal model

Temperature distribution through the fuel element is computed according to the conservation energy principle given by:

$$p \cdot C_p \cdot \frac{\partial T}{\partial t} = div\left(\lambda \cdot gradT\right) + p_v \tag{9.1}$$

with T the temperature, ρ the density, c_p the heat capacity, λ the thermal conductivity, and p_v the nuclear power density in the fuel.

The heat transfer through the pellet-to-cladding gap is derived from a Robin boundary condition (see Eq. 9.2) prescribed on the pellet external surface and cladding internal surface and added to the thermal stiffness matrix. The equivalent heat transfer coefficient h depends on: the local radial gap size, the gas composition in free volumes, the contact pressure, and interface contact roughness for a closed gap.

$$\Phi = h \cdot (T_{clad} - T_{pellet}) \tag{9.2}$$

with h the equivalent heat transfer coefficient of the gap, T_{clad} the cladding internal surface temperature, and T_{pellet} the pellet external surface temperature.

9.2.2.6.2 Mechanical model

Mechanical state of the fuel element is computed with the static equilibrium and its boundary conditions (see Eq. 9.3) integrated according a weak formulation with the Finite Element method.

$$\begin{cases} div\,\bar{\bar{\sigma}} = 0 \text{ in } \Omega \\ \bar{\bar{\sigma}}\,\vec{n} = \vec{\Sigma}_{imp} \text{ on } \partial\Omega_T \text{ such as, } \partial\Omega_T \cap \partial\Omega_u = \varnothing \text{ and } \partial\Omega_T \cup \partial\Omega_u = \partial\Omega \\ \vec{u}^{mec} = \vec{U}_{imp} \text{ on } \partial\Omega_u \end{cases} \tag{9.3}$$

where $\partial\Omega_T$ and $\partial\Omega_u$ are external surfaces with Neuman and Dirichlet boundary conditions, respectively.

In addition to this equilibrium principle, the nonlinear behaviors of the pellet and the cladding are taken into account through several mechanical models with a generic formulation based on the Hooke law and an additive formulation to compute the elastic strain rate as de difference between the total strain rate and all inelastic strain rates (see Eq. 9.4).

$$\dot{\bar{\bar{\sigma}}} = \underline{\underline{E}} : \left(\dot{\bar{\bar{\varepsilon}}}^{tot} - \dot{\bar{\bar{\varepsilon}}}^{th} - \dot{\bar{\bar{\varepsilon}}}^{ir} - \dot{\bar{\bar{\varepsilon}}}^{plast} - \dot{\bar{\bar{\varepsilon}}}^{creep} - \dot{\bar{\bar{\varepsilon}}}^{crack} \right) \tag{9.4}$$

where $\underline{\underline{E}}$ is the Hooke fourth order tensor, $\dot{\bar{\bar{\varepsilon}}}^{tot}$ the total strain rate, $\dot{\bar{\bar{\varepsilon}}}^{th}$ the thermal expansion strain rate, $\dot{\bar{\bar{\varepsilon}}}^{ir}$ the irradiation volumetric strain rate, $\dot{\bar{\bar{\varepsilon}}}^{plast}$ the plastic strain rate, $\dot{\bar{\bar{\varepsilon}}}^{creep}$ the creep strain rate, and $\dot{\bar{\bar{\varepsilon}}}^{crack}$ the inelastic strain rate induced by cracks extension.

The constitutive Eq. (9.4) lead to a nonlinear ODE system. In Alcyone and Germinal these equations are implemented with MFront. In the case of the Alcyone 3D computational scheme the following inelastic strains are introduced:

- isotropic thermal expansion in the pellet and anisotropic thermal expansion in the cladding
- isotropic densification induced by irradiation and mechanical compressibility in the pellet
- isotropic swelling induced by irradiation defects and gaseous FP in the pellet
- anisotropic swelling induced by irradiation defects in the cladding
- isotropic creep strain in the pellet, including three main contributions: athermal irradiation-induced creep, thermal creep[1] induced by void diffusion, and thermal creep (see footnote 1) induced by dislocation motion[2]
- crack strain in the pellet based on a smeared crack model [32,33]
- anisotropic thermal creep strain in the cladding including irradiation damage effects
- anisotropic plasticity strain in the cladding under high strain rate loading.

[1] Irradiation acceleration coefficient is prescribed to thermal creep to represent activation energy due to fission spikes.

[2] At high strain rate ($> 0.1\ s^{-1}$) the dislocation creep model is equivalent to a plastic behavior with no strain rate sensitivity.

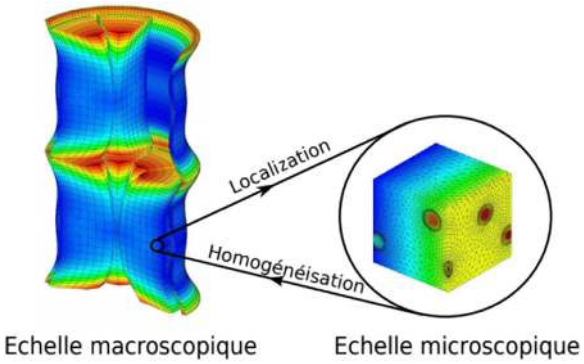

FIGURE 9.4 Computational scheme with the multiscale square finite element algorithm in ALCYONE.

9.2.2.6.3 Pellet-to-cladding gap model

The pellet-to-cladding gap is described with a finite element mesh based on joint elements for the thermal exchange and on solid-to-solid unilateral contact conditions for the mechanical behavior. The nonlinear mechanical solution gives the contact status opened or closed, with the gap size or the mechanical pressure, respectively, for all the nodes describing the gap. Then the thermal exchange coefficient through the gap (h in Eq. 9.2) can be assessed with the gap radial size as a function the circumferential and the axial positions. Thanks to the multiphysic convergence loop the contribution of the nonuniform gap size to the pellet temperature and to the pellet-to-cladding mechanical interaction can be computed.

9.2.2.6.4 Multiscale analysis

The ALCYONE multidimensional computational scheme includes also the finite element square multiscale approach [38] proposed as a generic algorithm in the PLEIADES architecture (see Section 9.1.2.1). In this approach, a 3D finite element model of a Representative Volume Element can be used to assess the nonlinear mechanical behavior at the microstructure scale. This multiscale computational scheme, illustrated on Fig. 9.4, is used for heterogeneous MOX fuel and can be extended to any kind of fuel heterogeneities.

9.2.3 3D simulation results and integral validation of the ALCYONE code

The mechanisms leading to pellet-cladding gap closure and ridge formation in the cladding during base irradiations and power ramp tests can be schematically decomposed as described later.

9.2.3.1 Base irradiation

During the first power increase the thermal gradient and associated fuel fragmentation are at the origin of the hourglass shape of the pellet (see Fig. 9.5). The consequence is a reduction of the gap at the interpellet (IP) plane (see Fig. 9.5A). Then, during the power hold period the fuel element dimensions will change due to the following phenomena:

- densification and solid swelling in the pellet and
- cladding creep under a compressive stress state

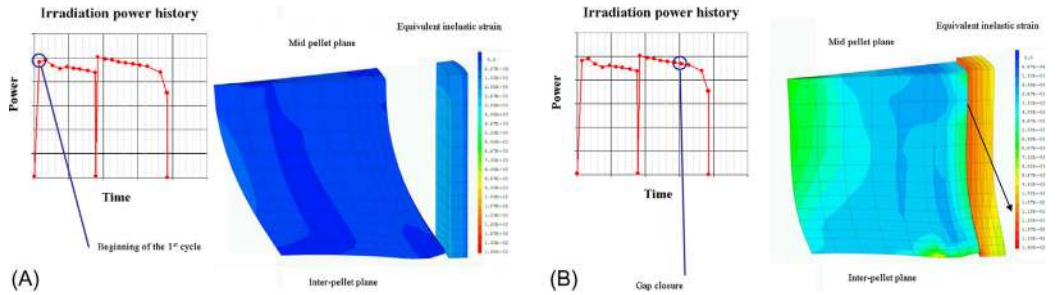

FIGURE 9.5 Pellet cladding gap closure and cladding ridging mechanisms under base irradiation: (A) hour glass shape at the end of the first power increase and (B) complete gap closure during the second cycle.

The competition between these geometrical changes leads to a gap decrease with mainly two steps of PCI:

- low interaction stage with a gap partially closed in the vicinity of the inter pellet plane and
- strong interaction stage with a gap entirely closed and a significant contact pressure level (see Fig. 9.5B).

During the interaction period the pellet hourglass shape is printed in the cladding because of its inelastic strains due to material creep under external pressure loading. Moreover, the cladding diameter decrease can also tend to reduce the extent of pellet hourglass magnitude, thanks to stress relaxation due to irradiation-induced creep in the pellet fragment. Through this analysis, it appears that the magnitude of cladding primary ridges at the end of base irradiation is the result of the competition between cladding and pellet creep. The development of a high-burn up structure in the pellets with pronounced gas-swelling can smooth the radial deformation of the cladding after base irradiation (see Ref. [9]).

9.2.3.2 Power ramp test

The behavior of fuel rods during ramp testing depends on many factors: the geometry of the fuel pellet (height/diameter ratio of the pellet, dish volume, chamfer dimensions, etc.), the power history (maximum power, increase of power, power rate, duration of holding period, etc.), the thermomechanical behavior of fuel and cladding (burn up of the pellet, thermal expansion of the fuel pellet, cladding creep and plasticity, fuel creep, etc.), and fission gas swelling in the fuel pellet (see Fig. 9.6).

The diameter increase of the cladding during power ramp is driven by the thermal expansion of the pellet and by fission gas swelling if the temperature of the pellet is high enough. The contribution of gas swelling can be important particularly if the holding period is long ($>20-30$ minutes) or if the fuel rod has a high burn up.

Cladding expansion during ramp testing is first induced at IP level due to the hourglass of the pellet resulting from the thermal gradient (see Fig. 9.6A) but soon it is compensated by dish filling due to creep and fission gas swelling of UO_2. If the height/diameter ratio of the pellet is large (>1.5), the impact of the dish filling on the creep strain accommodation at the MP plane will be small. Radial expansion will, therefore, be maximum at MP level since dish filling will limit radial expansion at IP level (see Fig. 9.6B). This is the reason why the MP ridges observed

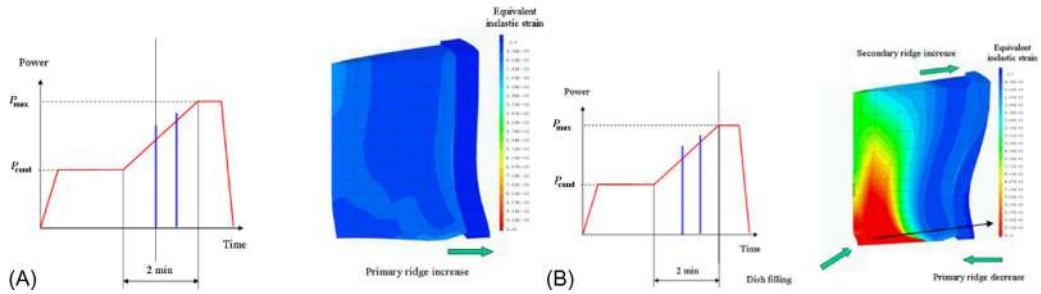

FIGURE 9.6 Pellet viscoplasticity and cladding ridging mechanisms under power ramp test: (A) primary ridge increase at the beginning of the power transient and (B) impact of viscoplasticity at the end of the power transient.

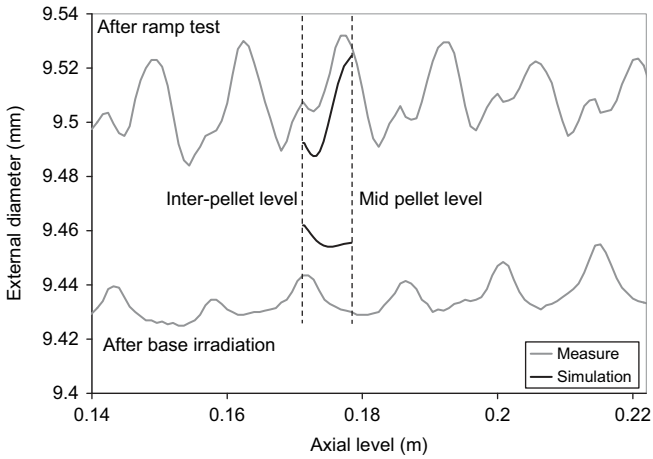

FIGURE 9.7 3D calculated and measured ridges after base irradiation and ramp testing showing the important development of the mid-pellet ridge during ramp testing. *3D*, Three-dimensional.

in the database can reach significant values (30 μm) and often exceed their IP counterparts by a factor 2 or 3, see Fig. 9.7. This is not the case with pellets of smaller height/diameter ratio (∼1) as was shown with ALCYONE 3D in reference [9] since dish filling has, in this case, consequences on the deformation of the MP plane due to axial creep. Hourglass-induced strains remain, therefore, predominant in this configuration leading mainly to IP ridges.

The integral validation of the ALCYONE code is based on around 340 study cases, presented in Table 9.2, with input data and postirradiation examination results stored in the CRACO experimental data base.

An illustration of the computation/measurement comparisons obtained for the integral validation of the 1D computational scheme of ALCYONE is given in Figs. 9.8–9.10 (see Ref. [5]). As shown in these figures, simulation results are well correlated to experiments for a large range of irradiation conditions. Computation-experiment gaps, generally centered on the perfect agreement curve, have been identified for the whole application domain and can be used to provide a conservative assessment or an uncertainty analysis.

TABLE 9.2 Study cases used for the integral validation of ALCYONE.

Fuel	Cladding	Irradiation conditions	Computational scheme	Number of study cases
UO_2/MOX	Zy4/M5	Nominal up to 80 GWd/t	Standard 1D	124
		PCI power ramp		37
UO_2/MOX		Analytical experiments		8
UO_2	Zy4/M5	Nominal up to 80 GWd/t	1D + MARGARET FGM	40
MOX				47
UO_2		PCI power ramp		22
MOX		Nominal	1D + RACHEL HGM	10
		PCI power ramp		2
UO_2	Zy4/Zirlo	LOCA	1D standard	2
UO_2/MOX	Zy4/M5	Nominal	2D and 3D standard	41
		PCI power ramp		
UO_2/MOX	Zy4/M5/Zirlo	RIA	1D and 3D	10

1D, One-dimensional; *2D*, two-dimensional; *3D*, three-dimensional; *PCI*, pellet-cladding interaction.

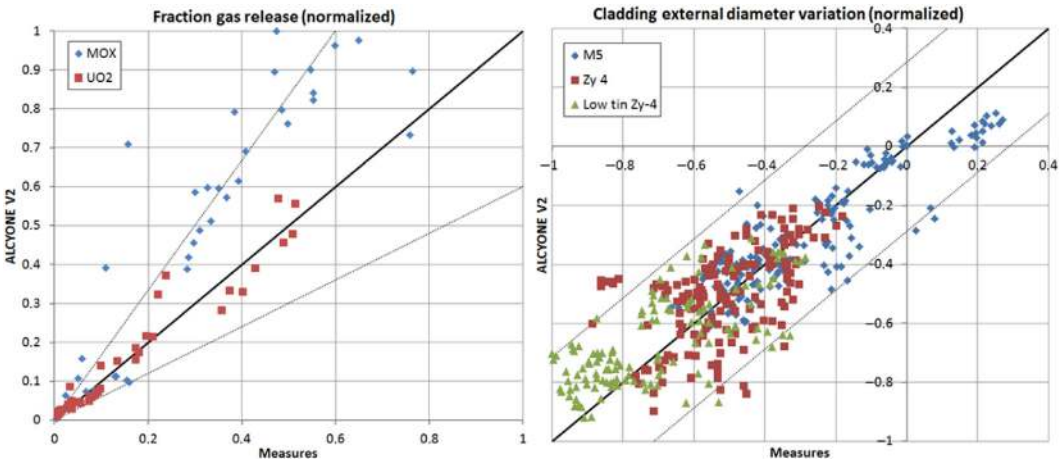

FIGURE 9.8 Fraction gas release (left) and cladding external diameter variation (μm) (right) at the end of base irradiation: ALCYONE 2.0 versus measures.

The integral validation of the ALCYONE 3D computational scheme has been done with three main types of experimental data: residual cladding ridges at the end of irradiation [39], pellet cracks density [40], and residual dishing volume [41]. An illustration of the simulation/experiment comparison is given on Fig. 9.11 for the pellet ridges at the end of base irradiation.

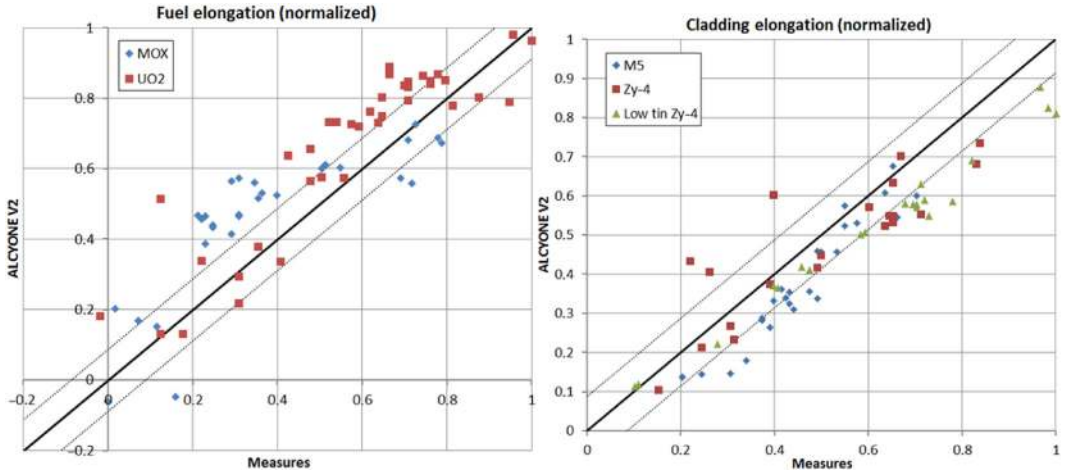

FIGURE 9.9 Fuel (left) and cladding (right) elongation at the end of base irradiation: ALCYONE 2.0 versus measures.

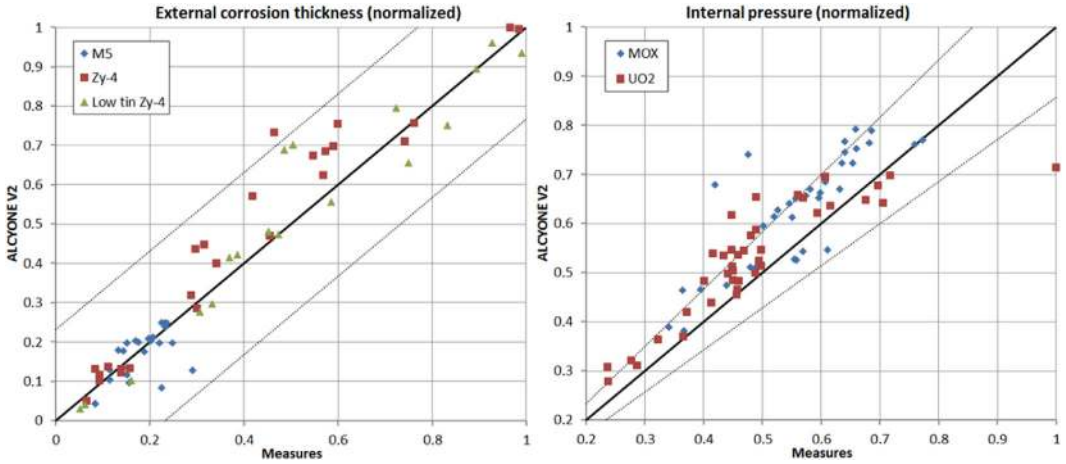

FIGURE 9.10 External corrosion thickness (left) and internal pressure (bar) (right) at the end of base irradiation: ALCYONE 2.0 versus measures.

The validation is still qualitative, but it gives important insights to understand the competition between different phenomena involved in the PCI.

Pellet dish filling validation is illustrated on the Fig. 9.12 with a simulation/experiment comparison given for various power-ramp test conditions. Thanks to this comparison, the influence of the pellet thermal creep law can be clearly understood. In Ref. [41] an inverse engineering method is proposed to fit the material parameters of the fuel irradiated creep law with the fuel dish filling measurement.

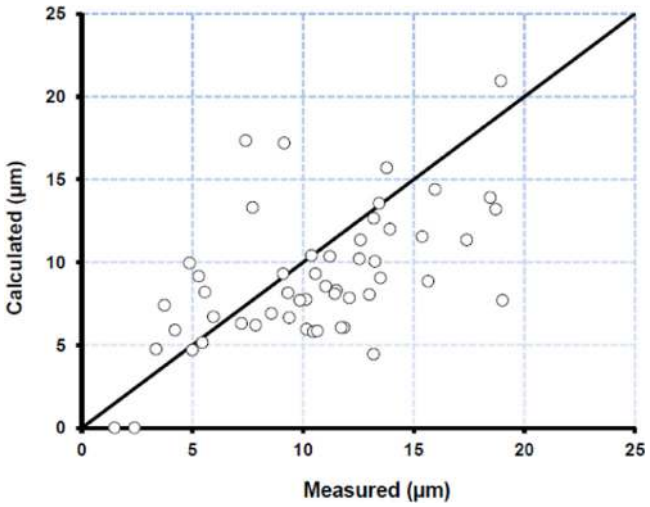

FIGURE 9.11 Calculated and measured heights of interpellet ridges at the end of base irradiation.

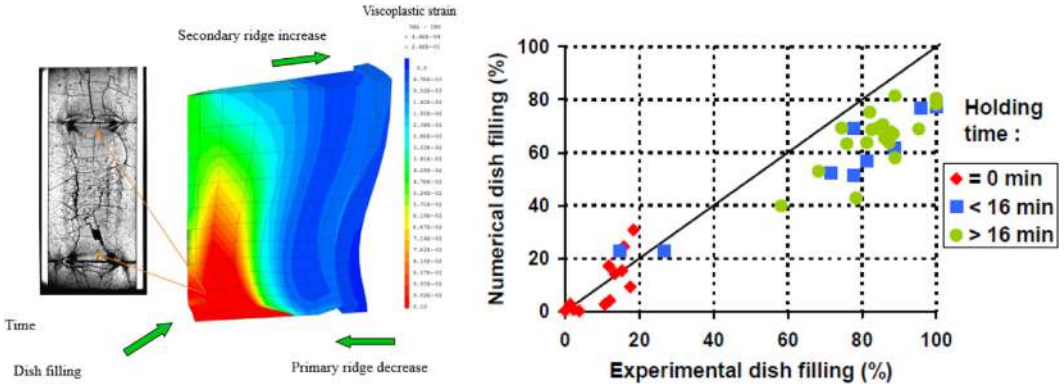

FIGURE 9.12 Calculated and measured dish filling after a power ramp test.

Fuel pellet radial crack pattern evolution and associated 3D simulations are illustrated on Fig. 9.13. Simulation and experiment are compared on the Fig. 9.14 as a function of the burn up. In reference [40] the number of cracks measurement was used to fit the pellet-to-cladding friction coefficient. Thanks to this inverse method, the crack density increase assessment as a function of the burn up is in good agreement with experimental values.

9.2.4 International benchmarks

The ALCYONE code has been benchmarked in the framework of several international program such as the SCIP project [9], the IAEA Concerted Research Project FUMAC [42], or the NEA Working Group Fuel Safety [43].

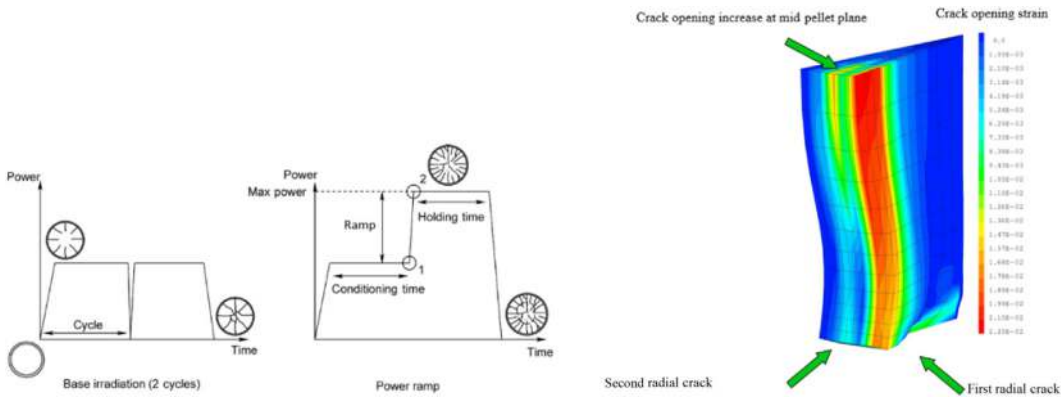

FIGURE 9.13 Irradiation history and pellet radial crack pattern evolution under normal and off-normal operating conditions.

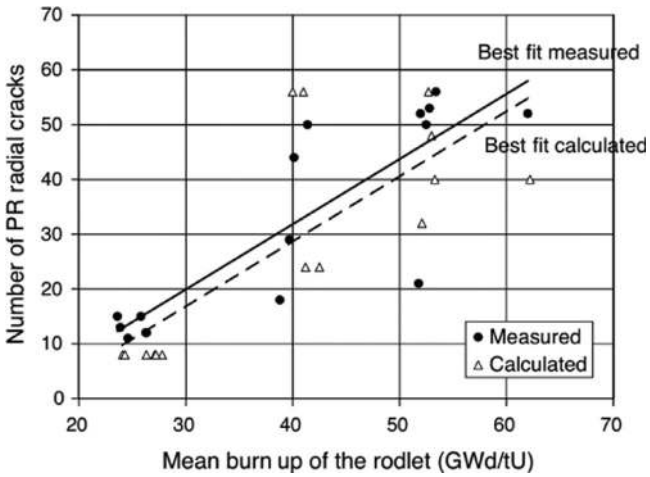

FIGURE 9.14 Calculated and measured number of radial cracks in the fuel pellet as a function of the fuel rod mean burn up.

9.3 GERMINAL fuel performance code for GEN IV

9.3.1 General presentation

The GERMINAL code [7] is dedicated to SFR fuel pin behavior under normal and off-normal operating conditions. The GERMINAL's computational scheme is based on the generic algorithm of the PLEIADES platform (see Section 9.1.2) with a local scale model based on the 1D axisymmetric geometrical assumption. The SFR multiphysics couplings are based on specific models of fuel behavior under high temperature and high fast neutron flux conditions (see Fig. 9.15). Among these physical aspects (all detailed in reference [7]), fuel restructuring, fuel pellet fragments relocation, and oxide-cladding joint [Joint Oxyde Gaine (JOG)] formation are briefly described in the following section. An advanced

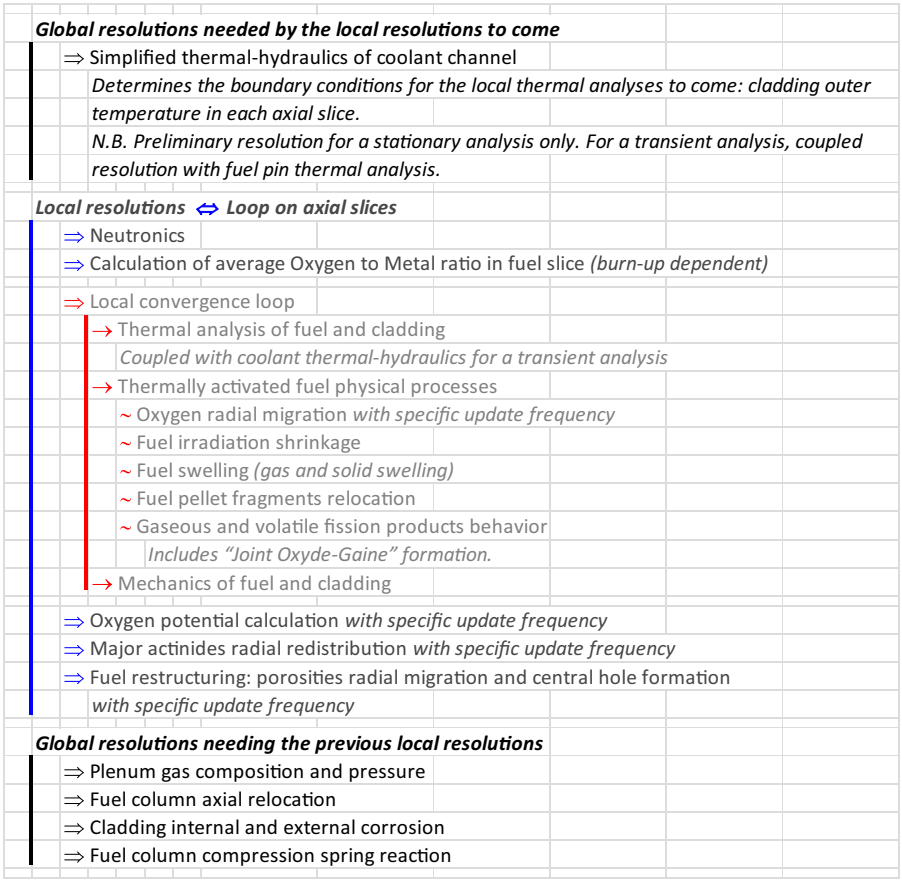

FIGURE 9.15 GERMINAL multiphysics computational scheme for one step [7].

modeling is under development for thermochemical aspects with a CALPHAD type thermodynamic computation coupled with the multiphysics algorithm and for pellet-to-cladding gap closure coupled with fuel restructuring and central hole formation

9.3.2 Physical models

9.3.2.1 Fuel restructuring

Fuel restructuring and associated central hole formation are due to high temperatures and steep radial thermal gradients occurring in SFR fuel pins—around 5000°C/cm in normal operating conditions [44]. The mass transfer inside fuel modifies the microstructure of the material and leads to geometry changes at the pellet scale. The driving physical process is pore migration toward the fuel center, activated both by the high temperatures and their radial gradient. Pore migration is due to an evaporation−condensation mechanism [45], where oxide molecules evaporate from the hottest free surface of a pore or a microcrack, then diffuse through

the gaseous phase and finally condense on the coolest free surface. Pore migration by vapor transport leads to form columnar grains along the way of the pores toward the pellet center, where the coalescence of the pores results in a central hole. This phenomenon usually happens at the beginning of irradiation—fresh fuel is the most reactive—but it is essentially depending on operating conditions that will fix the temperatures and their radial gradient [44,46,47]. A temperature threshold around 1800°C−2000°C is usually considered for the activation of the mechanism. It may also happen later in irradiation, as a consequence of an increase of reactor power or fuel-to-clad gap reopening due to irradiation-induced swelling of clad material. In GERMINAL the radial pore migration is described by the following advection equation:

$$\frac{\partial p}{\partial t} = -\frac{1}{r}\frac{\partial\left(r v_p p\right)}{\partial r} \tag{9.5}$$

where p is the fractional porosity ⇔ porosity volume ratio (dimensionless) and v_p is the average pore velocity (m/s).

The average pore velocity is derived from a microscopic model of the actinides vapor mass transfer through helium in a spherical pore [44].

In GERMINAL, Eq. (9.5) is solved from a finite volume integration method. The initial condition is a radially uniform porosity in the fuel pellet. The contribution of free volumes induced by the pellet fragmentation is derived from the relocation strain and added, at each time step, to the total porosity.

The central hole radius is deduced from the radial porosity versus time profile, corresponding to the upper bound of the domain where the porosity ratio is equal to one. The resolution of fuel restructuring also verifies the integral condition of mass conservation along the pellet radius, at all times.

9.3.2.2 Gap closure and relocation model

The fuel thermal power removal depends greatly on the heat-transfer coefficient in the pellet-to-cladding gap. At first order, this coefficient can be defined as the ratio of the average thermal conductivity coefficient of the gas mixture to the gap thickness. Heat conduction through solid−solid contact between pellet and cladding represents a contribution that is lowered when compared to that in a PWR fuel rod, since the fuel−clad mechanical interaction is itself lowered as a consequence of a low external pressure (coolant pressure) in an SFR. Hence, the gap size influences considerably the heat exchange between the fuel and the cladding and, consequently the fuel temperature changes. During irradiation the gap, initially filled with helium, is polluted by the FGR, leading to a decrease in the average thermal conductivity of the gap. This degradation of the gas mixture thermal conductivity is compensated by the gap size reduction, which finally induces a fuel temperature decrease. Then, in order to have a good assessment of the fuel maximum temperature at the beginning of life, the gap size effect on the thermal power removal has to be described in the multiphysics coupling. In GERMINAL the gap closure mechanism is described by a fuel fragments relocation model [7] combined with the pellet and cladding mechanical equilibrium. The fragments radial relocation is modeled with a uniform free strain in the plane(r, θ), according to the 1D axisymmetric geometrical assumption (local scale).

In the current version of GERMINAL an empirical formulation (see details in [7]) has been proposed in order to accurately describe the relocation displacement as a function of the thermal gradient in the pellet. The parameters of this relocation model have been fitted with an indirect validation of the maximal fuel temperature based on experimental measurements of the central hole radius and the restructured zone radius. Thanks to this model a good simulation/experiment agreement is obtained for solid and annular pellets under a large range of linear heat rates.

Recently, a new relocation model has been proposed in order to replace in the end the empirical formulation with physics-based constitutive equations. This formulation, presented in Ref. [48], considers two mechanisms to explain the relocation displacement:

- displacement increase of a fragmented pellet compared to an unfragmented pellet and
- radial displacement induced by the volume increase of the columnar grains zone.

The first mechanism is described by the mechanical equilibrium of a fragmented pellet compared to that of an unfragmented one. The second mechanism corresponds to the volume increase of the fuel restructured zone, resulting from the mass redistribution of the material that was originally located in the central hole. It is derived from a balance equation ensuring the mass conservation during the crack porosity migration contributing to the central hole formation.

9.3.2.3 Joint Oxyde Gaine formation and interaction with thermomechanical behavior

At high temperature the volatile FP (Cs, Te, and I) do not form stable compounds that would enable them to remain in the hot regions of the pellets. As they behave more or less like gas, a fraction of them migrates down the thermal gradient and condensates in the colder area at the periphery of the pellets in order to form a new phase called the "Joint Oxyde Gaine" (JOG [44]).

In the current version of GERMINAL, a JOG model based on the Cs release is proposed [7]. The Cs release is correlated to the stable FGR, itself derived from a single grain diffusion model. In this model the diffusion coefficient consists of two terms, including a thermal activation effect and an irradiation activation effect [7].

The equivalent thickness of fully dense JOG is estimated as the product of the released quantity of volatile FP and an average molar volume representative of the elements entering into the JOG composition.

In order to assess the real thickness of the JOG, a coupling with mechanical modeling has to be considered. If the pellet-to-cladding gap is greater than the equivalent JOG thickness, the JOG is assumed to be porous and its thickness is equal to the gap size. When the gap size is lower than the fully dense JOG equivalent thickness, the pellet-to-cladding contact condition is changed into a minimum gap condition, accounting for the initial gap size decreased by the fully dense JOG equivalent thickness. The pellet radius will then decrease under an accommodation process if some free volumes induced by pellet fragmentation (assessed with the radial relocation model described in Section 9.3.2.2) are still available. The formation of the JOG layer has also a significant impact on the heat transfer in the pellet-to-cladding gap and modifies consequently the fuel maximal temperature.

Some developments are in progress in order to improve the JOG composition assessment. In this new formulation the Calphad solver [13] available in the PLEIADES platform is used to compute the thermodynamic equilibrium in the pellet and in the pellet-to-cladding gap. The computational scheme under development has the following features:

- an estimation of the quantities of FP available in the fuel [18];
- a thermodynamic data base [27], including any chemical compounds which are likely to be involved in the JOG formation;
- a thermodynamic solver [13] to compute the inventory of the multiphase and multicomponent system as a function of the radius in the pellet and in the pellet-to-cladding gap;
- a simplified assessment of the release into the fuel-to-clad gap of gaseous chemical compounds available in the pellet; and
- an estimation of the JOG thickness and composition based on the thermodynamic equilibrium in the pellet-to-cladding gap.

First results have been obtained from this this new computational scheme and compared to experiments as presented in Ref. [49].

9.3.3 Validation and application for fuel design

9.3.3.1 Validation

Manufacturing features and irradiation conditions of fuel subassemblies and pins are stored in the BREF reference database together with postirradiation examination fuel pins results. BREF is the validation experimental database for fast reactor fuels. It gathers data from several thousands of characterized pins irradiated in sodium-cooled fast reactors, including a wide range of fuel element features. Experimental results come mainly from irradiations achieved in the Rapsodie, Phenix, PFR, and CABRI reactors, and also from other experimental facilities in the framework of international collaboration (see Section 9.3.4. Manufacturing and irradiation conditions data are used as input data for the GERMINAL code. The calculated output data are then compared to PIE results available in the database.

The integral validation of the GERMINAL code is based on a selection of more than 100 fuel pins with different geometrical configurations and irradiation conditions. A large range of parameters was then able to be tested in the GERMINAL code through this experimental data base, including the following ones: solid or annular pellets, homogeneous or heterogeneous fuel column, pellet composition (plutonium content and oxygen-to-metal ratio) and cladding material. The application field derived from the integral validation is given in Table 9.3 extracted from Ref. [7].

An illustration of the validation results as given in Ref. [7] is proposed in Fig. 9.16. The latter graph shows an overall good agreement between experiments and simulation with some discrepancies for few experiments under low power operating conditions. Some improvements are expected with new developments focused on experiments irradiated at intermediate power level [50].

TABLE 9.3 Application field for the GERMINAL fuel performance code.

Fuel			
Material		$(U, Pu)O_{2-X}$, $(U, MA)O_2$, UO_2	
Pellet geometry		Solid/annular	
Pellet ϕ_{ext}		[4.2 → 12.2] mm	
Pellet ϕ_{int}		[0 → 2.5] mm	
Initial Pu/M		[0 → 45]%	
Initial MA/M		[0 → 21]%	
As-fab. O/M		[1.926 → 1.999]	
As-fab. density		[85 → 98] %Dth	
Cladding			
ϕ_{ext}	[5.1 → 28.0] mm		
Materials	Austenitic steels: 316[a], cold work 15 − 5 Ti and AIM1 Inconel 706, Nimonic PE16 EM12, HT9		
Fuel pin			
Types	Homogeneous		
	Axial heterogeneous		
Operating conditions			
Normal operating conditions		Power transients (CRWA, TOP)[b]	
Linear heat rate	[50 → 590] W/cm	LHR max. (RIA)	→ 1300 W/cm
Clad nominal temp.	[550 → 700]°C	Pmax/Pn (Top)	→ 26.3
Damage	[0 → 155] dpa	Coolant temp.	→ 900°C
Burn up	[0 → 23.7] at.%		

[a]*Tempered 316, cold work 316, cold work 316 Ti.*
[b]*Control Road Withdrawal Accident Transient Over Power.*
MA, Minor actinides, Np and/or Am.

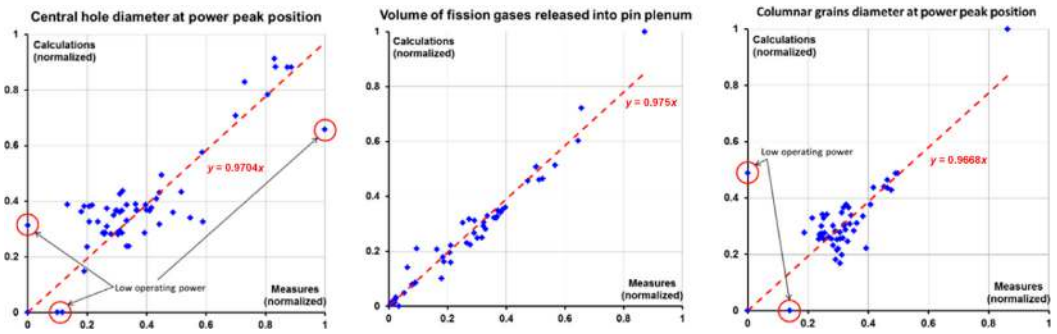

FIGURE 9.16 Illustration of the validation of GERMINAL.

9.3.3.2 Fuel design for the ASTRID project

The GERMINAL fuel performance code has been used in the framework of the conceptual design of the ASTRID fuel subassemblies [51]. The aim of this analysis was to check that the design criteria (maximal temperatures, mechanical constraints, clad swelling, etc.) are met in nominal and incidental transient conditions (CRW, etc.). A statistical analysis has also been proposed [52] to assess the number of pin failures during a severe accident.

9.3.4 International benchmarks

9.3.4.1 NEA expert group on innovative fuels

In the framework of the NEA Expert Group on Innovative Fuels group, fuel performance codes have been benchmarked with seven irradiations under normal operating conditions [53]. The following codes are compared: CEPTAR (JAEA, Japan), FEMAXI-FBR (KIT, Germany), GERMINAL (CEA), and TRANSURANUS (JRC-Karlsruhe) for oxide fuels; ALFUS (CRIEPI, Japan) and MACSIS (KAERI, Korea) for metal fuels. As an output of the benchmark conclusions were drawn in order to identify common understanding as well as discrepancies that require further investigation and developments. For oxides fuels analysis of the results from calculations (FGR, temperatures, fuel restructuring, and axial elongation) shows some discrepancies between the different codes. One of the most noticeable disagreements between the codes concerns the temperature predictions. This was attributed to the calculations performed on the gap size evolution, the gap heat conductance, and the evaluation of the fuel thermal conductivity. Improvement on models is, therefore, recommended to increase the accuracy of codes. In addition, the analysis revealed that the presence of a low content of MA in the fuel does not appear to be causing any significant differences in the codes calculations.

9.3.4.2 ESFR-SMART

In the ESFR-SMART European project code-to-code comparisons are provided for the computation of a fuel pin of an oxide core of 3600 MWTh with 15/15 TiCW cladding. The objective of this benchmark is to compare fuel performance code results regarding the design analysis of the fuel pins. The results, obtained with all the fuel performance codes, have been used to set a 2D correlation for the heat conductance with respect to fuel burn up and fuel rating [54].

9.3.4.3 CEA-JAEA collaboration

A cross-comparison between CEPTAR and GERMINAL was performed as benchmark calculations by both sides in accordance with the Fuel R&D collaboration objective. The latter is to improve the code validation database and to develop new fuel models. Irradiation experiments, selected for the benchmark calculations, are:

Two JOYO experiments devoted to measure the in-pile fuel center temperature and the power-to-melt

Two Phenix experiments devoted to solid and annular pellet under burn up levels of 11 and 9 at.%, respectively.

The results analysis has revealed similarities and differences between the two codes.

9.3.4.4 *INSPYRE European project*

In the framework of the INSPYRE project the GERMINAL fuel performance codes is benchmarked with TRANSURANUS and MACROS through some computation/experiment and code-to-code comparisons [55]. The main objective of this benchmark is to test new models and material properties derived from the basic research achieved in the INSPYRE project. For GERMINAL significant improvement are expected for the modeling of stable fission gas behavior, especially thanks to the implementation of the SCIANTIX module [56] in the GERMINAL code.

9.4 Conclusion and prospects

After 15 years of development the fuel performance codes ALCYONE and GERMINAL of the PLEIADES platform are fully operational for a use at an industrial stage. They offer standard and advanced multiphysic computational schemes with possible 1D−2D−3D and multiscale approaches. The PLEIADES software architecture used some open-source generic tools such as SALOME or MFront. The development and verification process have proven its flexibility and its robustness thanks to a continuous integration methodology. Fuel modeling and its validation with ALCYONE and GERMINAL capitalize results and knowledge of irradiation programs conducted for more than 40 years in PWR and SFR. These two codes have been benchmarked in the framework of various international collaborations, for which they have contribute to improve the understanding of fuel behavior under irradiation.

For several years the objectives have been focused on a detailed multiscale description in link with a separate effect approach in order to have a complete understanding of the mechanisms and the physical properties governing the fuel element behavior in the reactor core. These improvements, requiring small scale simulations, smart experiments, and high performance computations, will be the key for a better understanding, including uncertainties, needed for a safe and innovative design.

Acknowledgment

This work has been done in the framework of a cooperative program between CEA, EDF, and FRAMATOME.

References

[1] <https://www.salome-platform.org/>.
[2] <http://www-cast3m.cea.fr/>.
[3] T. Helfer, Introducing the open-source mfront code generator: application to mechanical behaviors and material knowledge management within the PLEIADES fuel element modelling platform, Comput. Math. Appl. 70 (5) (2015) 994−1023.
[4] C. Struzik, Validation of fuel performance CEA code ALCYONE, scheme 1D, on extensive data base, in: Proceedings of Top Fuel 2012, Manchester, United Kingdom, September 2−6, 2012, 2012.
[5] V. Marelle, Validation of PLEIADES/ALCYONE 2.0 fuel performance code, in: Proceeding of the Water Reactor Fuel Performance Meeting, 2017, Jeju, Korea.

[6] I. Guénot-Delahaie, Simulation of reactivity-initiated accident transients on UO_2-M5® fuel rods with ALCYONE V1.4 fuel performance code, Nucl. Eng. Technol. 50 (2) (2018) 268−279.
[7] M. Lainet, GERMINAL, a fuel performance code of the PLEIADES platform to simulate the in-pile behavior of mixed oxide fuel pins for sodium-cooled fast reactors, J. Nucl. Mater. 516 (2019) 30−53.
[8] Z. Jinzhao IAEA FUMAC Fuel Rod Code Benchmark, Uncertainty and Sensitivity Analysis on the Halden LOCA Tests, in: EHPG Meeting, 2019, Sandefjord, Norway.
[9] J. Sercombe, et al., 1D and 3D analyses of the Zy2 SCIP BWR ramp tests with the fuel codes METEOR and ALCYONE, Nucl. Eng. Technol. 41 (2) (2009) 187−198.
[10] Reactivity Initiated Accident (RIA) Fuel Codes Benchmark Phase-II, NEA/CSNI/R(2016)6/VOL1, March 2016.
[11] INSPYRE project, Work Package 7, 2017-2021, http://www.eera-jpnm.eu/inspyre/.
[12] I. Ramière, Th. Helfer, Iterative residual-based vector methods to accelerate fixed point iterations, Comput. Math. Appl. 70 (9) (2015) 2210−2226.
[13] B. Sundman, U.R. Kattner, M. Palumbo, S.G. Fries, OpenCalphad − a free thermodynamic software, in: Integrating Materials and Manufacturing Innovation vol. 4, no. 1, 2015.
[14] V. Marelle, New developments in ALCYONE 2.0 fuel performance code, in: Proceedings of Top Fuel 2016, Boise, ID, September 11−15, 2016.
[15] J. Sercombe, R. Masson, T. Helfer, Stress concentration during pellet cladding interaction: Comparison of closed-form solutions with 2D(r,θ) finite element simulations, Nucl. Eng. Des. 260 (2013) 175−187.
[16] B. Michel, J. Sercombe, C. Nonon, F. Michel, V. Marelle, Simulation of pellet-cladding interaction with the PLEIADES fuel performance software environment, Nucl. Technol. 182 (2013) 124−137.
[17] L. Noirot, MARGARET: a comprehensive code for the description of fission gas behavior', Nucl. Eng. Des. 241 (6) (2011) 2099−2118.
[18] F. Lemoine, D. Bernard, E. Federici, Validation assessment of neutron calculations for radial and azimuthal distributions of actinides and fission products in PWR rods, in: Presented at 2011 Water Reactor Fuel Performance Mtg., Chengdu, China, September 11−14, 2011.
[19] J. Noirot, L. Desgranges, J. Lamontagne, Detailed characterisations of high burn-up structures in oxide fuels, J. Nucl. Mater. 372 (2) (2008) 318−339.
[20] J. Noirot, Y. Pontillon, S. Yagnik, J.A. Turnbull, T. Tverberg, Fission gas release behaviour of a 103GWd/tHM fuel disc during a 1200°C annealing test, J. Nucl. Mater. 446 (1) (2014) 163−171.
[21] J. Noirot, Y. Pontillon, S. Yagnik, J.A. Turnbull, Post-irradiation examinations and high-temperature tests on undoped large-grain UO_2 discs, J. Nucl. Mater. 462 (2015) 77−84.
[22] J. Noirot, I. Zacharie-Aubrun, T. Blay, Focused ion beam−scanning electron microscope examination of high burn-up UO_2 in the center of a pellet, Nucl. Eng. Technol. 50 (2) (2018) 259−267.
[23] C. Sabathier, et al., In-situ TEM observation of nano-void formation in UO_2 under irradiation, Nucl. Instrum. Methods Phys. Res. Sect. B: Beam Interact. Mater. Atoms 326 (2014) 247−250.
[24] M. Bertolus, et al., Linking atomic and mesoscopic scales for the modelling of the transport properties of uranium dioxide under irradiation, J. Nucl. Mater. 462 (2015) 475−495.
[25] G. Jomard et al., CARACAS: An industrial model for description of fission gas behavior in LWR-UO2 fuel, in: Proc. of Water Reactor Fuel Performance Meeting/TopFuel Conference, Sendai, Japan, 2014.
[26] M.H. Piro, D. Sunderland, S. Livingstone, J. Sercombe, W. Revie, A. Quastel, K. Terrani, C. Judge, A review of pellet clad interaction behavior in zirconium alloy fuel cladding, Reference Module In Materials Science And Materials Engineering, Elsevier, 2017.
[27] C. Guéneau, et al., Thermodynamic modelling of advanced oxide and carbide nuclear fuels: Description of the U−Pu−O−C systems, J. Nucl. Mater. 419 (2011) 145−167.
[28] <https://www.oecd-nea.org/science/taf-id/>.
[29] B. Baurens, et al., 3D thermo-chemical−mechanical simulation of power ramps with ALCYONE fuel code, J. Nucl. Mater. 452 (2014) 578−594.
[30] P. Konarski, et al., 3D Simulation of power ramps with ALCYONE including fuel thermochemistry and oxygen thermodiffusion, J. Nucl. Mater. 519 (2019) 104−120.
[31] J. Sercombe, C. Riglet-Martial, B. Baurens, Simulations of power ramps with ALCYONE including fission products chemistry and oxygen thermo-diffusion, in: Pellet-Clad Interaction (PCI) in Water-Cooled Reactors, 2016 <https://www.oecdnea.org/nsd/docs/2018/csni-r2018-9.pdf>.

[32] B. Michel, 3D fuel cracking modelling in pellet cladding mechanical interaction, Eng. Fract. Mech. 75 (11) (2008) 3581−3598.
[33] B. Michel, A new numerical methodology for simulation of unstable crack growth in time independent brittle materials, Eng. Fract. Mech. 188 (2018) 126−150.
[34] J.M. Ricaud, R. Masson, Internal variables formulation of the effective behavior of linear viscoelastic heterogeneous media: exact and approximated results, Int. J. Solids Struct. 46 (2009) 1599−1606.
[35] V. Blanc, L. Barbie, R. Largenton, R. Masson, Homogenization of linear viscoelastic three phase media: internal variable formulation versus full-field computation, Procedia Eng. 10 (2011) 1889−1894.
[36] R. Masson, k. Sec, M.E.B., J. Fauques., M. Garajeu, A modified secant formulation to predict the overall behavior of elasto-viscoplastic particulate composites, J. Mech. Phys. Solids, Volume 137, April 2020, https://doi.org/10.1016/j.jmps.2020.103874.
[37] A. Bouloré, C. Struzik, R. Masson, R. Largenton, P. Mailhé, Approach to better assess fission gas behaviors, applicable to fuels with complex microstructures, in: 2017 Water Reactor Fuel Performance Meeting, Ramada Plaza Jeju, Jeju Island, Korea, 10−14 September 2017.
[38] F. Feyel, A multilevel finite element method (FE2) to describe the response of highly non-linear structures using generalized continua, Comput. Methods Appl. Mech. Eng. 192 (28−30) (2003) 3233−3244.
[39] J. Sercombe, 3D modelling of strain concentration due to PCI within the fuel code ALCYONE, in: TopFuel 2013, USA.
[40] J. Sercombe, I. Aubrun, C. Nonon, Power ramped cladding stresses and strains in 3D simulations with burn up-dependent pellet−clad friction, Nucl. Eng. Des. 242 (2012) 164−181.
[41] J. Julien Adjustment of fuel creep behavior based on post-ramp dish filling observations and 3D simulations: impact on clad ridges, in: Top Fuel 2012, UK.
[42] M. Veshchunov et al., FUMAC: IAEA's Coordinated Research Project on Fuel Modelling in Accident Conditions, in: Trans. TopFuel 2018, Prague, Czech Republic, 30 September−4 October 2018.
[43] NEA/CSNI/R(2018)9, Pellet-clad interaction (PCI) in water-cooled reactors, in: Workshop Proceedings, NEA Working Group on Fuel Safety (WGFS), Lucca, Italy, 22−24 June 2016.
[44] Y. Guérin, Fuel Performance of Fast Spectrum Oxide Fuel, in: Comprehensive Nuclear Materials, Vol. 2, pp. 547-578, 2012.
[45] P.F. Sens, The kinetics of pore movement in UO_2 fuel rods, J. Nucl. Mater. 43 (1972) 293−307.
[46] C.F. Clement, The movement of lenticular pores in UO_2 nuclear fuel elements, J. Nucl. Mater. 68 (1) (1977) 63−68.
[47] C.F. Clement, M.W. Finnis, The movement of lenticular pores in mixed oxide (U, Pu) O_2 nuclear fuel elements, J. Nucl. Mater. 75 (1) (1978) 115−124.
[48] M. Temmar, B. Michel, I. Ramiere, N. Favrie, Multi-physics modelling of the pellet-to-cladding gap closure phenomenon for SFR fuel performance codes, J. Nucl. Mater. 529 (2020) 151909.
[49] K. Samuelsson, J.-C. Dumas, B. Sundman, M. Lainet, An improved method to evaluate the Joint-Oxyde-Gaine formation in (U, Pu)O_2 irradiated fuels using the Germinal V2 code coupled to Calphad thermodynamic computations, EPJ Nuclear Sci. Technol. 6 (2020), https://doi.org/10.1051/epjn/2020008.
[50] I. Munoz-Viallard et al., Overview of axially heterogeneous PAVIX 8 fuel pin irradiation in PHENIX within the framework of the French GEN IV development program, in: Conference Proceeding Paper 29755, GLOBAL 2019, Seattle, WA, September 22−27, 2019.
[51] T. Beck, et al., Conceptual design of ASTRID fuel sub-assemblies, Nucl. Eng. Des. 315 (Apr. 2017) 51−60.
[52] V. Blanc et al., Fuel melting margin assessment of fast reactor oxide fuel pin using a statistical approach, in: Proc. of FR17, Yekaterinburg.
[53] N. Chauvin et al., Benchmark study on fuel performance codes for fast reactors, in: Conference GLOBAL 2019, September 22−27, 2019 Seattle, USA, paper 29755.
[54] J. Lavarenne et al., A -2D correlation to evaluate fuel-cladding gap thermal conductance in mixed oxide fuel element for SFR, in: Conference GLOBAL 2019, September 22−27, 2019 Seattle, USA, paper 30569.
[55] L. Luzzi et al., Development and assessment of a mechanistic model describing high burnup structure behavior in oxide nuclear fuel, in: NuFuel-MMSNF 2019 Workshop PSI, Villigen, 04 − 07/11/2019.
[56] D. Pizzocri, T. Barani, L. Luzzi, SCIANTIX Code, Online Repository. [Online]. Available: <https://gitlab.com/poliminrg/sciantix> (accessed 04.10.19).